5

Cathodoluminescence Properties of Zno Thin Films

M. Addou et al.[*]
University of Ibn Tofail
Morocco

1. Introduction

The industry has a great need for high performance materials to feature well defined. These needs have prompted the development of methods of study and control of gradually more sophisticated based on the radiation-matter interaction. To identify the properties of materials, we must make a spectral analysis on the emitted photon using a spectrometer combined with a detection system. The analysis of the photon can take place directly in the form of an electrical current, as well as the spectrum received by the measurement system is represented by a function I (λ).

The best radiations are the electrons because they are easy to produce, accelerate and to focus. In this context we speak of cathodoluminescence, which was long used in devices including fluorescent screens. This phenomenon, resulting from the excitation of luminescent materials by electron beam, is leading to photon emission, which is subject to the laws of the transitions. We usually distinguish the intrinsic luminescence (transition band to band, free exciton) and extrinsic luminescence from impurities and defects. The most common application is the television screen (when it is a cathode ray tube). In geology, the cathodeluminescence microscope is used to examine internal structures of geological samples in order to determine, for example, the history of rock formation. Another important application is Cathodoluminescence in image mode. In this mode the cathodoluminescence can view the spatial distribution of responsible levels for a radiative transition observed or locate the non radiative defects such as dislocations, grain boundaries and precipitates. These defects give rise to a generally strong contrast. It is possible to determine the energy levels that are at the root of this contrast. So we used this technique to study the nature and distribution of defects and impurities in materials [1].

Semiconductors exhibit energy gap between the valence band and the conduction band, the order of the electron volt. An incident electron beam of sufficient energy can move electrons from the valence band to the conduction band, thus producing electron-hole pairs; return to the ground state can be achieved through nonradiative transitions or by radiative transitions with photon emission of light. This return is via two mechanisms (direct recombination and

[*]J. Ebothé, A. El Hichou, A. Bougrine, J.L. Bubendorff, M. Troyon, Z. Sofiani, M. EL Jouad,
K. Bahedi and M. Lamrani
University of Ibn Tofail, Morocco

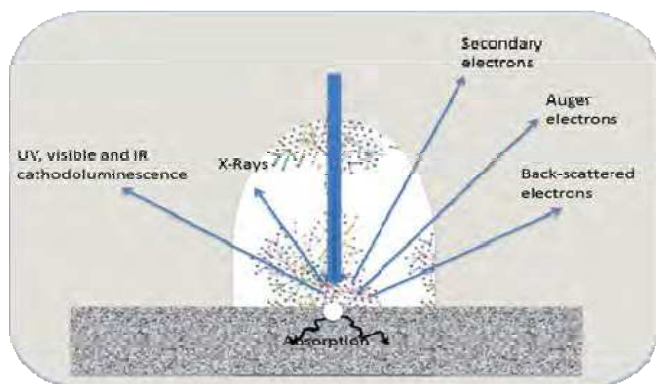recombination indirect). The CL signal is formed by detecting the photons in the UV, visible and IR.

Fig. 1. Cathodoluminescence schema

1. The region of high energy loss (DE> 50eV) corresponding to the excitation of deep levels K, L,… creates the X and Auger radiations.
2. The region of low energy loss (DE <50eV) corresponds to the excitation of the valence and conduction (photon CL).

The most important mechanisms in the analysis of CL in semi-conductors are:

- Electron-solid interaction.

- Dissipation of energy.

- Generation of carriers (e-h).

From the experimental point of view, a study of CL can be simplified to an electron gun, a sample and a detector.

Many parameters are involved and contribute to enhance the cathodoluminecence intensity during the growth process. Temperature effect, doping effect, flow rate deposition effect and the excitation energy effect are strongly among many other parameters, which influence the optical properties of thin films. The investigation on their luminescence remains very limited, especially the cathodoluminescence. However, band-edge photoluminescence in polycrystalline ZnO has not received as much attention as the bulk material because the band-edge photoluminescence is usually weaker and lacks the fine structure of the bulk crystals. Nevertheless, a study of the photoluminescence structure of this material is interesting, because it can provide valuable information on the quality and purity of the material. Polycrystalline films may also have different photoluminescence mechanisms as compared to the bulk material.

A^{II}–B^{VI} compounds, such as transparent and conducting oxides films, have been attracting ample attention as starting material for electro-luminescent devices because of their high visible transmittance and low electrical resistivity in the visible region. Zinc oxide (ZnO) is one of the few metal oxides, which can be used as a transparent conducting material. It has some advantages over other possible materials such as In_2O_3–Sn, $CdSnO_4$, or SnO_2, due to its unique combination of interesting properties: non-toxicity, good electrical, optical and piezoelectric behaviour, high stability in a hydrogen plasma atmosphere and its low price [2,3]. So, ZnO is a good candidate to substitute indium tin oxide (In_2O_3:Sn) and tin oxide (SnO_2), in conductive electrodes of amorphous silicon solar cells.

Furthermore, ZnO has the same crystal structure as GaN: wurtzite crystal structure and direct wide band gap. It is closely lattice matched to GaN. ZnO therefore offers potential as a substrate material on which high quality GaN may be grown. The room temperature band gap of ZnO is 3.3 eV with emission in ultra-violet (UV) region. An outstanding feature of ZnO is its large excitonic binding energy of 60 meV leading to the existence and extreme stability of excitons at room temperature and/or even higher temperatures [4-7]. These characteristics have generated a wide series of applications for example, as gas sensors [8], surface acoustic devices [9], transparent electrodes [10] and solar cells [3] among others. The preparation of zinc oxide thin films has been the subject of continuous research. Many techniques are used for preparing this transparent conductive ZnO such as: RF sputtering [11], evaporation [12], chemical vapour deposition [13], ion beam sputtering [14] and spray pyrolysis [15–18]. Among these methods spray pyrolysis has attracted considerable attention due to its simplicity and large scale with low-cost fabrication. Additionally, by using this technique one can produce large area coatings without the need of ultra high vacuum.

Different process parameters of the intrinsic and doped ZnO films by spray technique have been published [19–22]. The investigation on their luminescence remains very limited, especially the cathodoluminescence. However, band-edge photoluminescence in polycrystalline ZnO has not received as much attention as the bulk material because the band-edge photoluminescence is usually weaker and lacks the fine structure of the bulk crystals [23,24]. Nevertheless, a study of the photoluminescence structure of this material is interesting, because it can provide valuable information on the quality and purity of the material [25]. Polycrystalline films may also have different photoluminescence mechanisms as compared to the bulk material.

This Chapter will be divided on three parts. The first one describe the effects of different process parameters such as substrate temperature, air flow rate and precursors of undoped ZnO films prepared by spray pyrolysis on glass substrate. Several cathodoluminescence bands and the corresponding emission processes are identified. It is also shown that SP is an adapted technique to achieve ZnO films with a quality comparable with that of transparent conducting oxide thin films prepared by other techniques.

The second one concerns some results of a systematic investigation of the crystallinity, the surface morphology, optical properties and the cathodoluminescence measurements of the undoped and Sn-doped ZnO thin films deposited by SP. Several CL bands and the corresponding emission process are identified.

The last section of this chapter is dealing with, the luminescence of the investigated ZnO samples is examined accounting for the effects of two main parameters: the Er dopant concentration and the incident electron beam energy. A general sight of the CL material behavior is first reported, which precedes a more refined study including the spectral peak's integration and the near-field imaging aspects.

2. Effect of deposition temperature (Ts), air flow rate (f) and precursors on cathodoluminescence properties of ZnO thin films

Earlier work indicated that ZnO exhibited three bands of luminescence are centered around 382, 510 and 640 nm, labeled near UV, blue-green and red bands, respectively [26–28]. Our undoped ZnO films displayed the same three cathodoluminescence bands. However, the relative intensities and the disappearance of the blue-green and red emissions depend strongly on the precursor and deposition conditions such as flow rate and/or substrate temperature and doping nature.

2.1 Variation of substrate temperature

Fig. 2 shows the cathodoluminescence of ZnO thin films, at E=5 keV electron beam energy with a beam current of about 1 nA, deposited at different substrate temperatures and different flow rates. The substrate temperatures (Ts) were varied from 350 to 500°Cwith an interval of 50°C, and with a flow off=5 ml/min. When the substrate temperature increases, the surface of our films is entirely covered by grains and condensed.
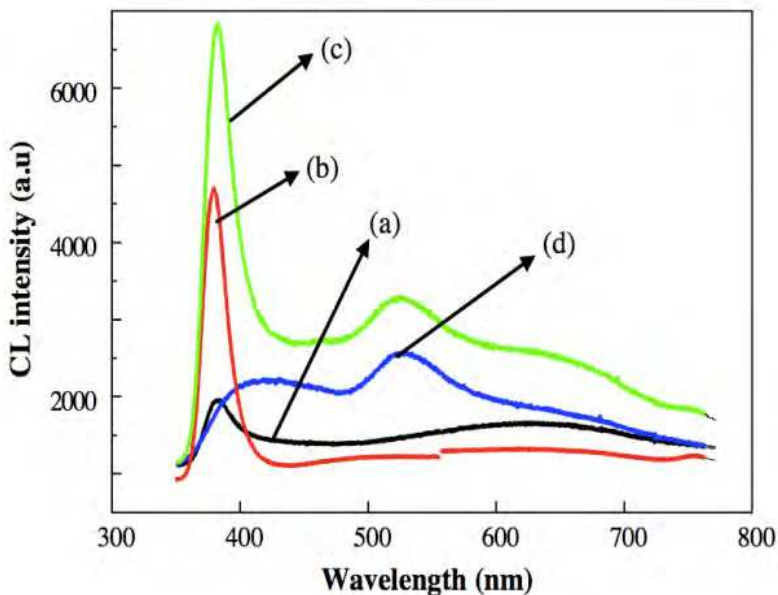

Fig. 2. CL Spectra of ZnO sprayed at flow rate f=5ml/min deposited on different temperature: (a) : T= 350°C, (b): T= 400°C, (c) : T= 450°C, and (d) : T= 500°C.

As indicated, the luminescence intensity depends strongly on the deposition temperature. Extinction of the blue-green emission (centered around 510 nm) is observed at substrate temperature of 350 and 400°C, whereas the near UV emission at 382 nm becomes more dominant than other transitions (blue-green and red emissions) at 450°C. The blue-green emission (510 nm) appears above substrate temperature 450°C but the red emission (640 nm) appears at different substrate temperature. At Ts=500°C, the UV transition shifts to higher wavelength and becomes comparable in cathodoluminescence intensity with blue-green emission. The maximum value of cathodoluminescence intensity for three bands is obtained at T=450°C.
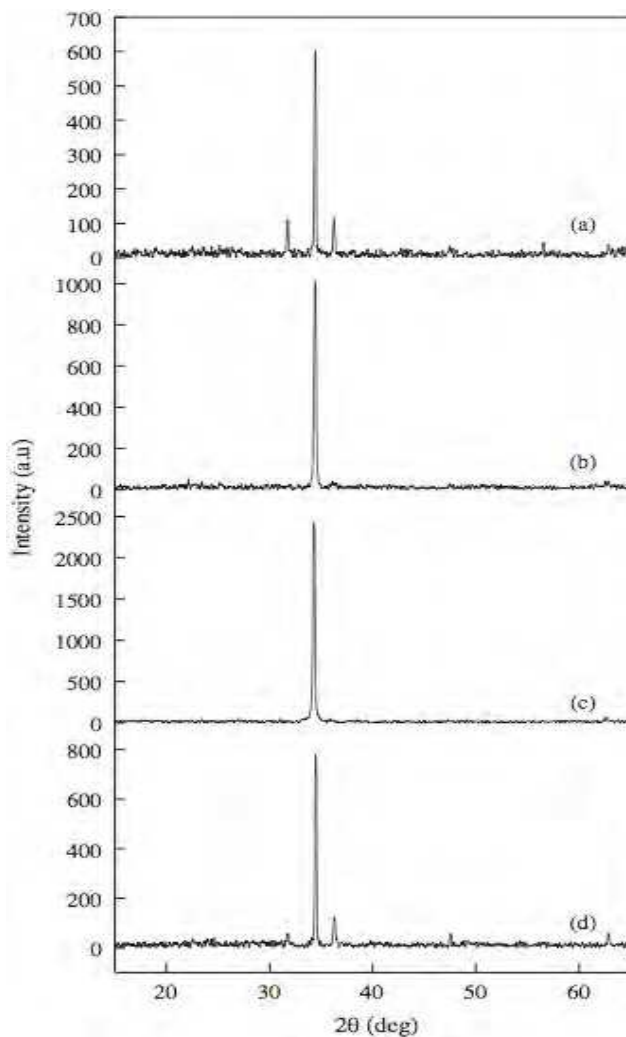

Fig. 3. XRD of ZnO sprayed at flow rate f=5ml/min deposited on different temperature: (a) : T= 350°C, (b): T= 400°C, (c) : T= 450°C, and (d) : T= 500°C.

Before discussing the cathodoluminescence observations of the films in more detail, it is useful to consider their crystal structure and morphology. The XRD of ZnO films, deposited at different substrate temperatures and at flow rate 5 ml/min, indicated that they possess a hexagonal close packed structure (Fig. 3). Moreover, it is the only main peak obtained with all films indicating that the increasing of substrate temperature does not change the preferred textural growth orientation. The [0 0 2] direction corresponds to the c-axis of the crystal lattice that it's normal to the deposition substrate plane. The XRD intensity depends strongly on the deposition temperature. The narrow range of deposition temperature permitted for maximum XRD intensity is illustrated by the pronounced peak at Ts=450°C.

The mean crystallite size D was calculated from the (0 0 2) diffraction peak using Scherrer's formula [29]. Values of D are listed in Table 1 for films prepared under various substrate temperatures. The mean crystal diameter was around 30 nm for the sample deposited at Ts=450 °C which was larger value as compared to all samples. We conclude that the films, which present strong cathodoluminescence intensity in UV emission, have a strong XRD intensity and large grain size, therefore a good crystallinity. We confirmed our results by using SEM images. Fig.4 clearly shows that there is a change in the surface morphology of ZnO films due to a change in the substrate temperature. It is evident that the porous structure occurred throughout the films deposited at Ts=350 °C (Fig. 4(a)). All films deposited at Ts>350 °C attain a microstructure and had a close-packed morphology. The films deposited at Ts=450 °C consists of hexagonal-like grains of approximately 300 nm size. The mean crystal diameters obtained using Scherrer's formula are all case substantially smaller than the dimension of grains observed by SEM image, indicating these grains are probably an aggregation of crystallites. The enhancement of cathodoluminescence intensity at substrate temperature 450°C could be due to a large grain size therefore a better crystallinity. The best luminescence was achieved with samples grown at T=450°C.

Substrate temperatures: T_s (°C)	350	400	450	500
Grain size: D (nm)	27.5	30	31.31	28
CL intensity of UV emission (arb.units)	2000	4700	6800	2100

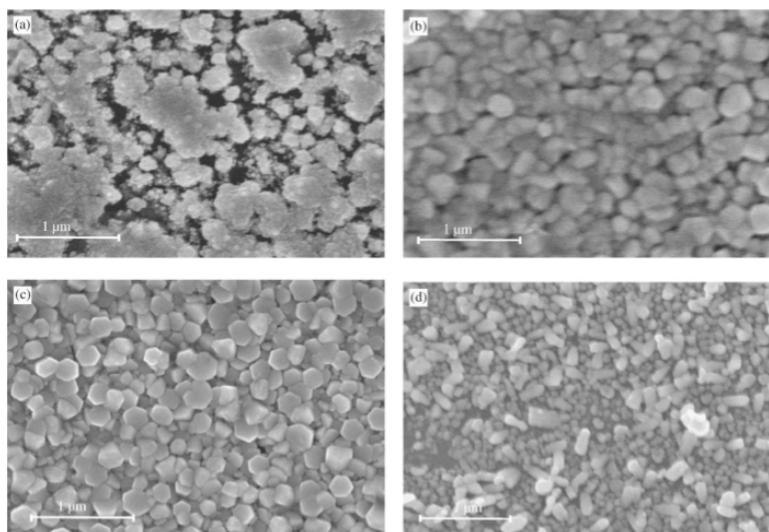Table 1. Grain size values at different substrate temperatures calculated using Sherrer's formula (f=5 ml/min)

Fig. 4. Morphology of ZnO sprayed at flow rate f=5ml/min deposited on different temperature: (a): T=350°C, (b): T= 400°C, (c) : T= 450°C, and (d) : T= 500°C.

2.2 Variation of airflow rate

The structural and luminescence properties of ZnO thin films are also investigated by varying the flow rate in the region 2.5pfp7.5 ml/min, which here is equivalent to the varying growth rate range of 0.2pro1 mm/s. This formation occurs on a deposited substrate made of soda glass whose temperature is fixed at Ts=450°C. Note that no cracks are observed on large scan area for all samples (SEM images Fig. 6). The films are continuous and in fact consist of grains. The cathodoluminescence spectra of these films (E=5 keV electron beam energy with a beam current of about 1 nA) at different airflow rate and at Ts=450°C are shown in Fig.5. For f=2.5 ml/min, one large band centered at 400 nm have been observed. When the spray rate enhanced, three emissions have been appeared with a dominance of the blue-green emission (510 nm) for f=3.75 ml/min and a strong intensity of the UV transition (382 nm) for f=5 ml/min. Furthermore, the appearance of the UV emission corresponds to the improved crystal quality. At high flow rate f46.25 ml/min, a degradation of cristallinity leads to decrease of the intensity related to UV transition and disappearance of both emissions situated in blue-green and red ranges.
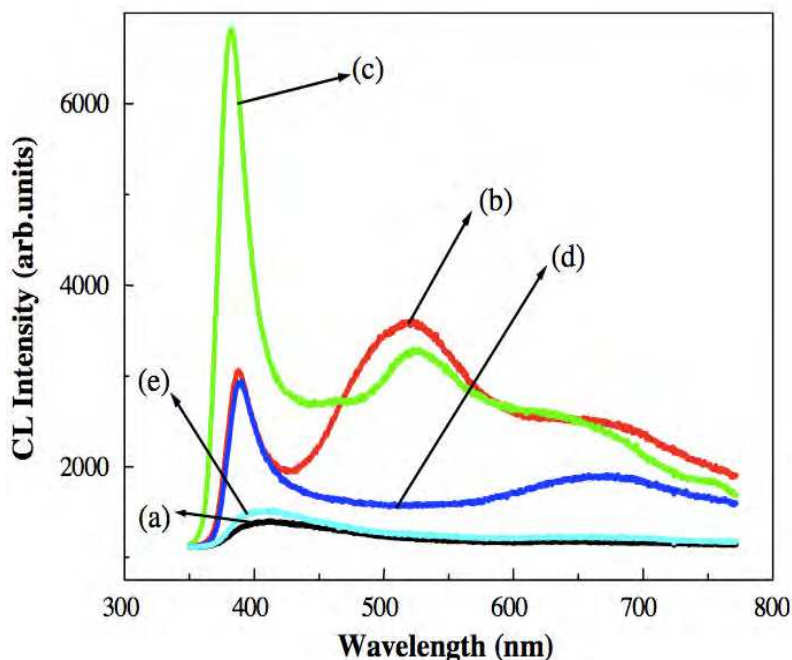
Fig. 5. CL Spectra of ZnO deposited at 450°C for different flow rate : (a) : f= 2,5ml/min, (b) : f= 3.75ml/min, (c) : f= 5ml/min, (d) : f= 6.25ml/min and (e) : f= 7.5ml/min

In Table 2, we have reported the mean grain size of ZnO films at different flow rate (statistical analysis of more than 100 grains on SEM images, Fig. 6). The some behavior of our samples at different substrate temperatures has been observed. Indeed, the low cathodoluminescence intensity of the UV transition is observed for films indicate small grain sizes and porous structure. We can conclude, that good crystallinity and the best luminescence are achieved with samples grown at f=5 ml/min. The decrease in surface grain size with the flow rate beyond f=5 ml/min appears to be mainly the effect of the non-incorporation of Zn particles on the material surface. The optimum flow rate and substrate temperature are f=5 ml/ min and Ts=450 °C, respectively. The films produced exhibit optical characteristics comparable to films grown by more sophisticated techniques.

Air flow rate f (ml/ min)	2.5	3.75	5	6.25	7.5
Grain size D (nm)	200	275	300	260	225
CL intensity of UV emission (arb.units)	1400	3100	6900	3000	1500

Table 2. Grain size calculated from SEM images at different air flow rates (T=450 °C)
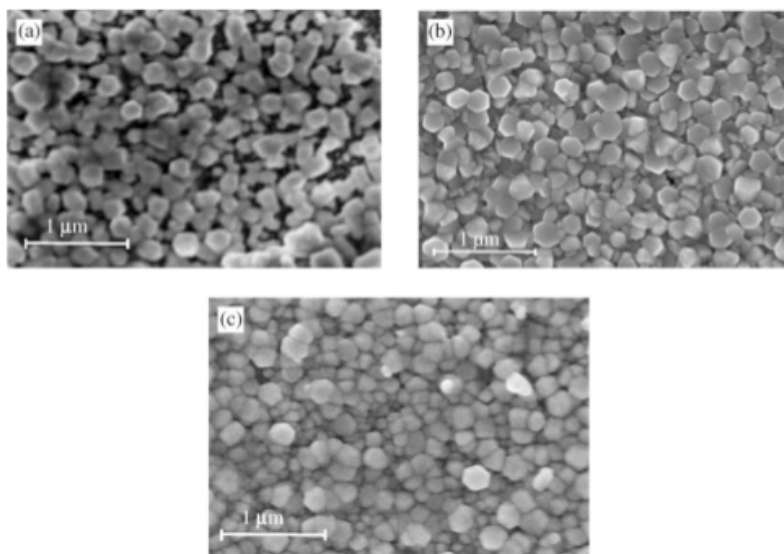
Fig. 6. SEM micrographs of ZnO films sprayed at substrate temperature Ts=450 °C and different air flow rate: (a) f=2.5ml/min, (b) f=5 ml/min, (c) f=7.5 ml/min and substrate temperature: Ts=450 °C.

2.3 Cathodoluminescence properties and variation of precursor

Cathodoluminescence spectra obtained from samples deposited at optimum condition Ts=450 °C and f=5ml/min is shown in Fig. 2(c). The three main emissions had peaks at 382, 520 and 672 nm. The luminescent at 382 nm corresponds to the band gap transition of ZnO. The presence of this band is an indicator of the good crystallinity.

The second peak centered at 520 nm is the characteristic of blue-green emission, which is also typical for ZnO material. Despite the numerous reports on the photoluminescence and cathodoluminescence of undoped ZnO, the luminescent centre responsible for this emission is not yet clearly identified. Several assumptions are proposed. Dingle [30] ascribes this emission peak to a substitution of Zn^{2+} by Cu^{2+} in the crystal lattice. According to Vanheusden et al. [31] and Egelhaaf et al. [23] this peak corresponds to a defect-related luminescence (deep-level luminescence), due to the oxygen vacancies in ZnO. This defect-related luminescence is explained by radiative transitions between shallow donors (oxygen vacancies) and deep acceptors (Zn vacancies). In this case, the acceptor level is located 2.5 eV below the conduction band edge [23,32], while the donor level is known as a shallow level at 0.05–0.19 eV, leading to an emission band centered around 508–540 nm. Furthermore, Minami et al. [33] proposed that the blue-green emission in this material might be associated to a transition within a self-activated centre formed by a double-ionized zinc vacancy $(V_{Zn})^{-2}$ and a single-ionized interstitial Zn^+ at the one and /or two nearest-neighbor interstitial sites. Nevertheless, the composition studies of our films by XPS and EDX analysis do not reveal presence of copper and thus the first explanation must be rejected. Therefore, one of the two other hypotheses may explain the blue-green emission that we observe.
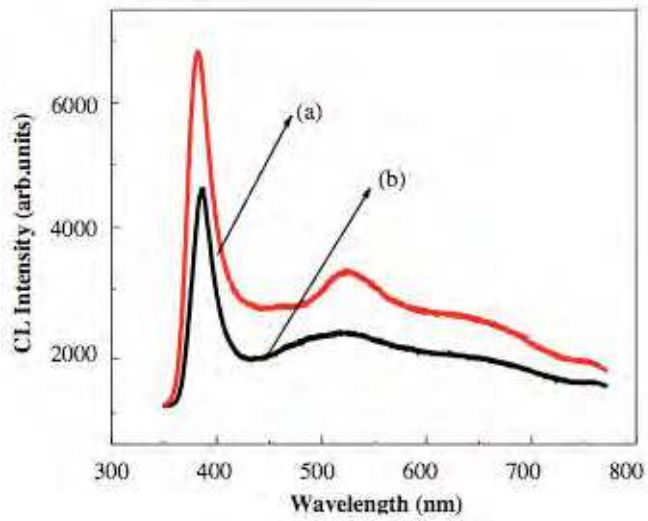
Fig. 7. Cathodoluminescence spectra of ZnO for both precursors (Ts=450 °C and flow rate f=5 ml/min): (a) $ZnCl_2$ and (b) AcZn

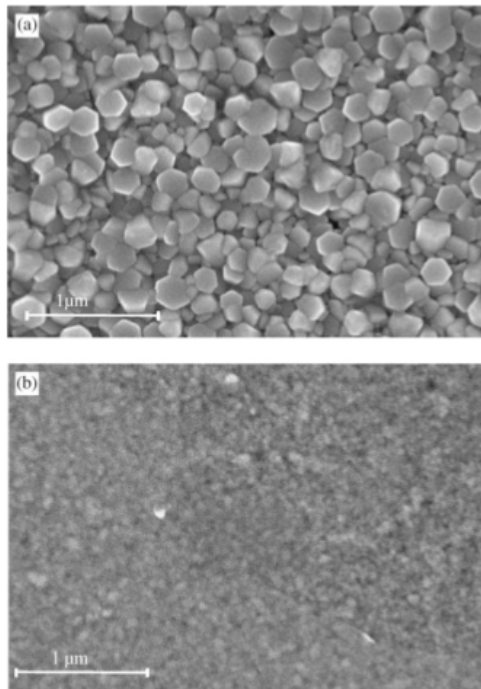Fig. 8. SEM micrographs of ZnO at different precursors (Ts=450 °C and flow rate f=5 ml/min: (a) ZnCl2 and (b) AcZn.

Previous works have also attributed the blue-green emission to a luminescent centre formed by the association of a doubly ionized zinc acceptor vacancy defect and of halogen impurities such as Cl atom of precursor. Fig.7 shows the cathodoluminescence spectra of undoped ZnO thin films preparing using zinc chloride ($ZnCl_2$) and zinc acetate (AcZn) as precursors. The presence of blue-green emission for both precursors is not attributed to the presence of chlorine atom, but confirms the attribution of blue-green emission to a self-activated centre. Furthermore, the SEM image of both samples shows there is a change in the surface morphology due to the presence of Ac or Cl atoms (Fig.8). The films prepared from precursor $ZnCl_2$ presents a better cathodoluminescence intensity, which confirms our choice for precursor, and the good cristallinity related to a dense structure and crystallites size relatively important. Cathodoluminescence intensity is directly correlated to an improvement of the films crystallinity.

The last peak at 670 nm, which appears markedly broad for this low beam energy (5 keV), may be due to the defect related deep emission, as shown by photoluminescence [34,35]. Lohnert et al. [36] pointed out that the intensity of broad luminescence observed from about 450 to 700 nm depends on the oxygen partial pressure in the sintering process of ZnO ceramics. This also suggests the hypothesis of a transition within a V_o^x neutral and single-ionized oxygen V_o^-.

2.4 Summary

The dependence of cathodoluminescence properties of spray-deposited ZnO films on process parameters such as substrate temperature, airflow rate and precursors, has been studied in detail. We have found that the luminescence intensity depend strongly on process parameters. The optimum values of substrate temperature and airflow rate have been determined to give the best luminescent ZnO films.

In the process of this investigation, it has been observed that the films are polycrystalline and have a preferred orientation in the [0 0 2] direction. The best films in terms of cathodoluminescence consisted of close-packed grains. These grains were an aggregation of many crystallites having a mean diameter around 30 nm.

The cathodoluminescence analysis of the sample deposited at optimum conditions (Ts=450 °C; f=5 ml/min) shows three bands: a near ultra-violet emission at 382 nm, a blue-green emission at 520 nm and a weak red one at 672nm.

3. Cathodoluminescence of undoped and tin-doped ZnO thin films

Cathodoluminescence (CL) spectroscopy, X-ray diffraction and spectrophotometery have been studied of undoped and tin (Sn)-doped ZnO films prepared by spray pyrolysis (SP) technique of zinc chloride and tin chloride. The luminescence films had a polycrystalline hexagonal wurtzite type structure. At room temperature, the cathodoluminescence (CL) spectra of the undoped and doped ZnO films exhibit the common near ultra-violet (UV) band-gap peak at $\lambda = 382$ nm but they differ as regards their visible emissions. The undoped ZnO emits an intensive blue–green light ($\lambda = 520$ nm) and a red emission ($\lambda = 672$ nm). The presence of tin gives rise to a new light emission corresponding to $\lambda = 463$ nm and the extension of blue–green light typical of the intrinsic behavior of the material. CL imaging of

undoped ZnO films show that the luminescence is located at defined sites giving rise to a grain-like structure inherent to the surface morphology. The presence of tin in the material leads to great luminescent spots, attributed to large grain sizes.

3.1 Experimental procedure

The luminescent films were prepared by spray pyrolysis using air as the carrier gas atmospheric pressure. The apparatus used for deposition is described and schematized elsewhere [37/21]. The spraying solution was prepared from a mixture of 0.05 M zinc chloride ($ZnCl_2$) and deionised water. A small amount of chloridric acid HCl was added in the solution to prevent the formation of zinc hydroxide ($Zn(OH)_2$). The nozzle is directed towards a substrate with a spraying flow rate of 5 ml/min. This substrate is made of bare glass sheets whose temperature is maintained constant at T = 450°C, that is known to be the optimal condition for this material formation. The same film thickness of 0.4 mm, estimated from the deposition time, is retained. A good agreement is obtained with the value deduced from the cross sectional images obtained by transmission electron microscopy. Tin doping was achieved by adding $SnCl_2$ to spraying in a concentration of 6 at.%. The compositionnal analysis of the films as performed with an EDAX 9100 analyzer indicates that the 6% tin percentage of the spraying bath is quite recovered in the Sn-doped ZnO samples.

The crystalline structure was investigated by X-ray diffraction using CuK radiation. Optical transmittance measurements were performed with a Shimadzu 3101 PC UV-VIS-NIR spectrophotometer. The cathodoluminescent (CL) spectra and images were measured at room temperature, using a LEO-GEMINI 982 scanning electron microscopy (SEM), operated from 1 to 30 kV and equipped with a field emission gun. Our CL system, in association with a spectrometer (Triax 190 from JOBIN YVON), allows monochromatic CL imaging as well as acquisition of CL spectra on very localized spots of a sample. The mechanical details of our homemade SFM microscope, implemented inside the SEM, are reported in [37]. In this paper, the photons enter directly a multimode optical fiber (numerical aperture = 0.48) leading to far-field images or spectra. The CL images are acquired with a fixed electron beam, the sample being scanned under the fiber. The spectrometer has a spectral resolution of 0.5 nm and is equipped with an N2-coolled CCD detector. Monochromatic CL images can be obtained by selecting a defined wavelength and by sending the light to a photomultiplier (PM, R4220P from Hamamatsu). The signal is then amplified with an electrometer and images of 256 × 256 pixels at a line frequency of about 0.1 Hz are generated. Panchromatic images are also obtained by directing the light towards the PM without passing through the spectrometer.

3.2 Results and discussion

X-ray diffraction patterns for undoped and Sn-doped ZnO thin films prepared at optimum parameters are shown in Fig.9. The diffraction (0 0 2) peaks located at the angular position 2θ = 34.4° (undoped ZnO) and 2θ = 34.38° (Sn-doped ZnO) are characteristics of the hexagonal close packed structure of this material. Moreover, it is the only main peak obtained with both films indicating that the presence of tin in ZnO keeps unchanged the preferred textural growth orientation. The (0 0 2) direction corresponds to the crystal lattice that is normal to the deposition substrate plane. It should be pointed out that the peak's

intensity of the Sn-doped ZnO films in Fig.9 (b) is higher that the one of the undoped sample of Fig.9 (a), it is full width at half maximum (FWHM) being broaded. One deduced that the doped sample has a better crystallinity. Probably, there is the substitution of oxygen by tin anions in the material sites, leading to a partial healing of the crystal network.
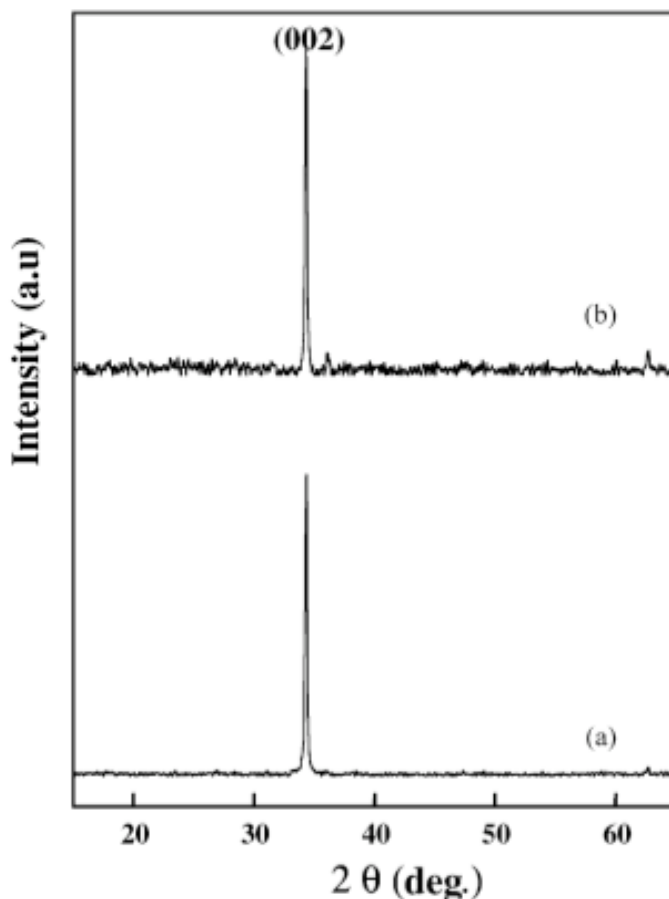

Fig. 9. X-ray diffractograms of: (a) undoped and (b) Sn-doped ZnO films.

Fig.10 consists of SEM showing the effect of doping on the surface morphology. We can see that the morphology evolves considerably after doping our samples. The undoped film in Fig.10 (a), depicts a microstructure consisted of hexagonal-like grain of approximately 200 nm size, the substrate surface being entirely covered for the film thickness retained. The last remark remains valid for the Sn-doped sample image of Fig.10 (b). Where as Sn-doped film presents a plate-like grains with polycristalline-like irregular grains. The size of the grains is larger (350 nm) and not uniform. Therefore, the crystallinity of Sn-doped ZnO films was significantly improved with Sn-doping. This is in a good agreement with X-ray diffraction results.
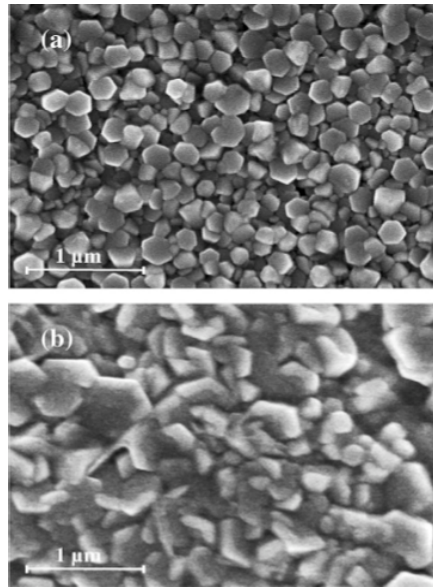
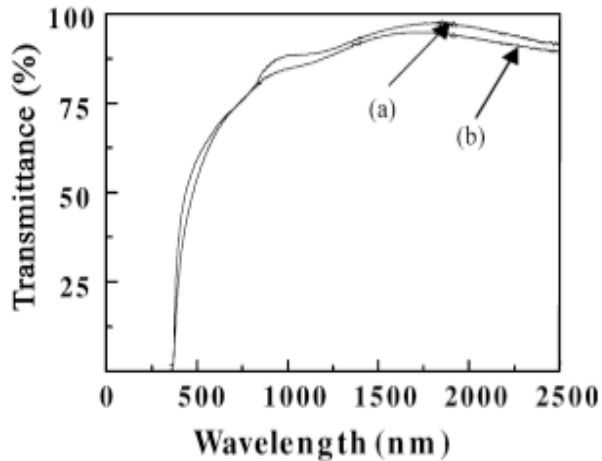Fig. 10. SEM micrographs of: (a) undoped and (b) Sn-doped ZnO films.

Fig. 11. Optical transmission spectra of: (a) undoped and (b) Sn-dopedZnO films.

The optical properties of undoped and Sn-doped films are restricted to their transmission spectra (Fig.11). The films were highly transparent above 85% in the visible wavelength range. For wavelengths in the absorption edge region, it is observed that it is shifted towards lower wavelengths. This effect has been already observed and discussed by other authors [38], significant an increasing in band-gap value. The results from the previous figures show that the ZnO film with good crystallinity and purity can be obtained by SP.
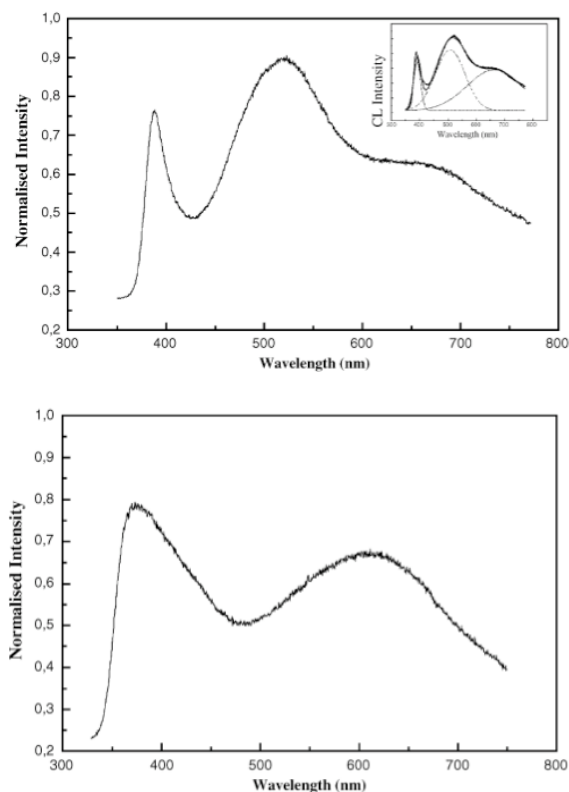
Fig. 12. Cathodoluminescence spectra of: (a) undoped ZnO and (b) Sn-doped ZnO films at E=5 keV electron beam energy with a beam current of about 1 nA.

Cathodoluminescence studies exhibit interesting features. In Figure 12, we present the cathodoluminescence emission spectra of undoped (Fig.12 (a) and Sn-doped ZnO thin film (Fig.12 (b)) at the electron beam energy of 5 keV. Early work indicated that ZnO exhibited three photoluminescence bands centered around 380, 520, and 650 nm, labeled near-ultraviolet (UV), blue–green and red bands [39,27,28]. Our undoped ZnO films displayed the same three cathodoluminescence emission, showing in Fig.12 (a). The first peak localized at $\lambda = 382$ nm (Eλ = 3.25 eV) corresponds to the band-gap transition of this material. It is clear that the appearance of the band-edge correspond to the good quality and crystallinity of our films and confirms the previous X-ray diffraction observations. The second peak of the undoped sample is the blue–green emission located at $\lambda = 520$ nm (Eλ = 2.38 eV) that is here typical of ZnO material. The luminescent center responsible for this emission is not clearly identified. It is ascribed by Dingle [30] to a substitution of Zn^{2+} by Cu^{2+} in the crystal lattice. Recently, it has been proposed that the blue green emission in this material might be associated to a transition within a self-activated center formed by a double-ionized zinc vacancy V_{zn}^{2-} and the single-ionized interstitial Zn^+ at the one and/or two nearest-neighbor interstitial sites [39,33]. According to Vanheusden et al. [31], the green–yellow luminescence (deep-level luminescence) is related to the oxygen vacancies in the grown ZnO crystals.

Egelaaf and Oelkrug [45] reported that those defect-related luminescence are caused by radiative transitions between shallow donors (related to oxygen vacancies) and deep acceptors (Zn vacancies). The acceptor level (Zn vacancies) is located 2.5 eV below the conduction band-edge [40,32], while the donor level is known as shallow as 0.05–0.19 eV. In our undoped ZnO samples, no copper impurities were detected using electron probe microanalysis (EPMA) and still we observe the blue–green emission. Therefore, it is likely that the blue–green emission observed in our samples might be better explained by the second hypothesis. The third peak at λ = 672 nm (Eλ = 1.84 eV), which appears markedly broad for this low beam energy, may due to the defect related deep emissions. Lohnert and Kubalek [41] pointed out that the intensity of broad luminescence observed from about 450 to 700 nm depend on the oxygen partial pressure in the sintering process of ZnO ceramics. This also suggests the hypothesis of a transition within Vo x neutral and single-ionized oxygen V_o^-.

The emission spectrum for the Sn-doped films, using electron beam energy of 5 keV, is a broad band composed of two peaks at 372 and 672 nm (Fig.12 (b)). The incorporation of Sn apparently results in a competitive phenomenon that overshadows the blue–green emission. This behavior could be originated by a more favorable transmission from the localized state generated by the Sn or could be due to a reduction of the self-activated centers responsible for the blue–green emission by occupation of the Zn vacancies by Sn ions. This figure confirms the shift of absorption edge observed by optical results.
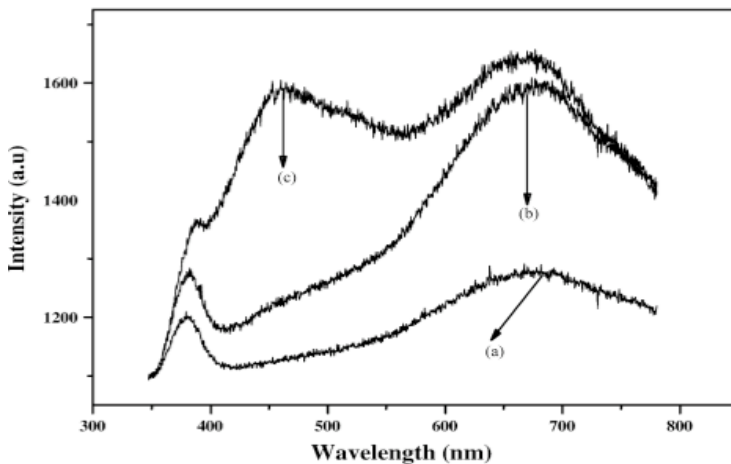

Fig. 13. Cathodoluminescence emission of Sn-doped ZnO films at different electron beam energies: (a) E = 7 keV, (b) E = 10 keV and (c) E = 15 keV.
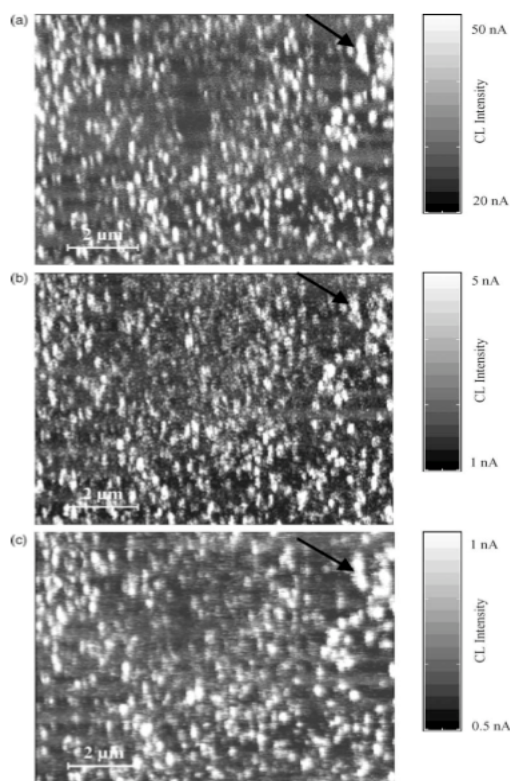
Fig. 14. Cathodoluminescence images of undoped ZnO thin film taken at E = 3 keV: (a) polychromatic CL image, (b) monochromatic CL image taken at λ = 382 ± 8 nm, (c) monochromatic CL image taken at λ = 520 ± 8 nm. The full arrow in each image is a marker for the investigated region of the film surface area.

Fig.13 represents the CL study of the Sn-doped sample at different electron beam energies (E = 7, 10, and 15 keV) proposed for investigating the material homogeneity versus the penetration depth of the electrons. It is clearly appeared that the predominant emission depends strongly by excitation. Indeed, at low excitation alone the tow peaks situated at 372 and 672 nm are observed. The peak localized at 372 nm is due to a transition band-gap with an increasing in band-gap value witch is due to tin doping. From 10 keV a new peak centered at 465 (Eλ = 2.66 eV) began to appear. This emission, that seems typical of tin element, may be associated with a complex luminescent center like (VZn –SnZn)−. At 15 keV, the peak at 465 nm becomes comparable in intensity with the peak situated at 672 nm. Therefore, the increase of this peak's intensity with E means that the tin concentration is higher in the bulk. This result has been verified by X-ray photoelectron spectroscopy (XPS) measurements after successive etching treatment of the sample surface. A similar investigation of the undoped ZnO film has shown that the intensity of the three peaks proportionally increases with the increase of E, implying that the SP deposition method can lead to the formation of homogeneous samples.

Figs. 14 and 15 show polychromatic and monochromatic images of the undoped and Sn-doped ZnO films obtained at the exciting beam energy E = 3 and 5 keV, respectively. The monochromatic images were recorded by selecting the appropriate wavelength with a spectral bandwidth of 16 nm. The CL images of undoped ZnO films (Fig.14) show that the luminescence is located at defined sites giving rise to a grain-like structure inherent to the sample morphology. In view of the relatively low exciting beam energy E = 3 keV, the lateral resolution of the CL images is noticeable. It is smaller than the mean grain size and approximates 100 nm, indicating that the diffusion length of the undoped ZnO film is of this order of magnitude or even smaller. Both monochromatic images at λ = 382 and 520 nm are not much different indicating that the luminescent centers responsible for the band-edge and the blue–green emissions are approximately located at the same places. Nevertheless, in Fig. 6(b), the monochromatic image corresponding to the band-edge emission is presented. A higher density of emitting sites, with smaller luminescent spots than those of Fig. 6(c).
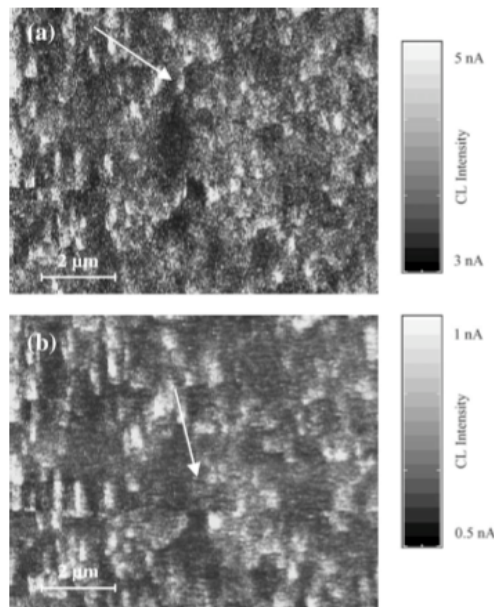

Fig. 15. Cathodoluminescence image of F-doped ZnO thin film taken at 4 keV: (a) polychromatic CL image, (b) monochromatic CL image taken at λ=372±8 nm. The full arrow in each image is a marker for the investigated region of the film surface area.

The CL images of Sn-doped ZnO films (Fig.15) show that the emission is less uniform, appearing more as a granular structure, with a greater luminescent spots than that of the intrinsic ZnO. The grain-like structure cannot be resolved by CL due to the finite carrier-diffusion length. Such a modulation of emission intensity would be attributed to areas with varying grain density, in which the bright regions corresponding to dense grains. Only a few luminescent defects, indicated by arrows on the images, are present. Notes that it is very difficult to take the monochromatic image at λ = 465 nm, because this emission appears at higher exciting beam energy.

In order to study, the effect of Sn doping on the properties of ZnO, we have plotted in Fig.16, the luminescent evolution versus different level doping at a single electron beam energy E = 5 keV. We have remarked a disappearance of bleu green emission observed in undoped ZnO even if level doping and peak intensity becomes more important when level doping increases.
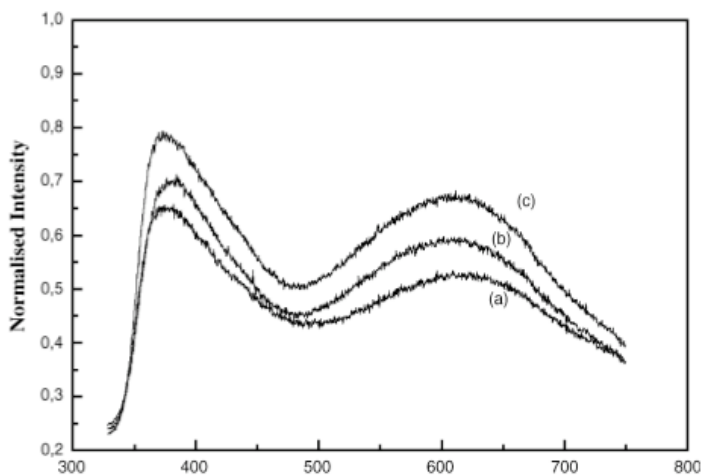

Fig. 16. Cathodoluminescence emission of Sn-doped ZnO films at different level doping: (a) 2 at.%, (b) 4 at.% and (c) 6 at.%.

3.3 Conclusion

Structural, optical and cathodoluminescence characteristics of sprayed ZnO films have been studied here. The effects of tin dopant at the atomic percentage of 6% on these film properties have been analyzed. The hexagonal wurtzite structure of the material is not modified by the presence of the Sn-dopant. The preferred (0 0 2) growth orientation of the films is not affected while an improvement of the material crystallinity is observed with this dopant. The cathodoluminescence analysis of the samples shows that the undoped film presents three bands: a near UV emission at $\lambda = 382$ nm in the near UV region, a blue–green emission at $\lambda = 520$ nm and a weak red one at $\lambda = 672$ nm. Incorporation of tin extinguishes the blue–green band while appears a blue light at $\lambda = 465$ nm and increases the value of the band-gap transition. CL imaging analysis shows that the repartition of the emitting centers in the material is intimately connected to the film morphology. The presence of tin in the material leads to great luminescent spots, due to large grain sizes.

4. Cathodoluminescence of undoped and Erbium-doped ZnO thin films

4.1 Introduction

The present work proposes an examination of erbium species influence on the visible and near UV luminescence of thermally sprayed ZnO-Er films. As shown elsewhere, the conditions used for this large scale and cheap deposition technique greatly affect the emitting characteristics of the undoped specimen. Hence, our first objective is the right

monitoring of the formation process for this matrix material from which the doping effect can be safely investigated. A particular attention is paid to the structure and composition evolution that mostly remain the basic origin of changes in materials physical properties. The use of rare earth elements as lanthanides engenders more complex phenomena resulting from a combined optical effect of both ZnO and the dopant shell as shown for embedded Er^{3+} species investigated nowadays for planar wave guides in telecommunication applications. In that case, ZnO host appears an excellent amplifier of the Er3+ intra-4f transition signal engendering an infrared line of 1.55 μm wavelength. This somewhat relegates from the time being to minor importance the role of these species in the near UV and visible emissions of ZnO thin films. Despite of it, some works are done here and there in this direction. The study of the lifetime decay in the green fluorescence observed with thermally annealed (Er^{3+}/Si^{4+})-ZnO nanocrystalline films was proposed by Kohls et al. [42] The room temperature blue luminescence of Er-doped ZnO thin films was also investigated by Zhang et al. [43] from samples prepared by simultaneous evaporation of ZnO and Er materials. It clearly appears in most of these reports that only expensive doped Er-ZnO films are involved in this research area. The cathodoluminescent characteristics of the samples in the near ultraviolet and visible region depict a complete extinction of the visible emitted bands (λ =445, 526, and 665 nm) at 1 at. % Er content. Their deactivation below this concentration is explained by a compensation of oxygen defects in the material due to the oxygen-rich medium of the deposition bath. Their reactivation beyond this particular concentration is ascribed to the increase of the Er^{3+} ion shells whose internal radiative transitions lead to a recovering of these visible emitted bands. The radiative mechanism of the transitions from the $^4F_{9/2}$ excited states to then $^4I_{15/2}$ ground state, responsible for the λ =665 nm emission, is predominant in that case. The respective normalized intensity of the violet λ =445 nm and green λ =526 nm emitted bands exhibits a maximal value for 3 at. % Er content, reaching a stabilized regime from about 5 at. % Er.

4.2 Experimental and characterization

Varying Er concentration in ZnO matrix, as proposed in the present work, requires some precautions due to the possible formation of a ternary compound. In actual fact, the physical solubility of Er in ZnO has not yet been clearly evaluated. Due to the high atomic weight of this dopant, this solubility is expected to be somewhat reduced. This necessitates a chemical and structural examination of our investigated samples in the limits of the selected doping concentration interval going till 10 at. %. In these conditions, the proposal of cathodoluminescent study could be done in the light of any change in the material composition and crystal phase.

4.3 Microstructure and composition of ZnO samples

Figure 17 reports the results of x-ray analysis obtained from three representative investigated specimens. As shown, one sees that the material depicts in every case a (002) diffraction peak corresponding to $2\theta = 34.5°$ angular position, which is a characteristic of the hexagonal close packed structure of ZnO $c_0 / a_0 = 1.6024$. This result implies that the related (002) direction, normal to the substrate plane, is the preferential growth orientation in every case. Figure 17(a) clearly reveals that this is the only main orientation of the undoped sample. One sees in Figs.17 (b) and 17(c) that the increase of erbium concentration

progressively modifies the film's textural feature with the appearance of two supplementary peaks of the same lattice at $2\theta = 31.8°$ and $2\theta = 36.3°$ that are, respectively, related to the 100 and 101 directions. It should be pointed out that this textural change occurs without any shift in the angular position of 002 diffraction peak and hence with no strain in ZnO matrix structure. A refined analysis of these results reveals that the dependence of the individual intensity of both peaks on the Er content quite differs.

Figure 18 shows that the intensity of the (100) peak always remains higher than the (101) one, regardless of the Er content. However, the (100) peak is more sensitive to the dopant presence particularly for the concentration higher than 5 at. % Er from which the 100 peak becomes markedly enhanced while only a slight increase of the (101) peak's intensity is observed. It should be noted that no typical peak of erbium or Er_2O_3 materials appears in the x-ray diffraction pattern of the films even for 10 at. % Er content. This ultimately gives an indication on the chemical nature of the investigated ZnO films and hence ensures on the real role of Er species in the material CL characteristics.
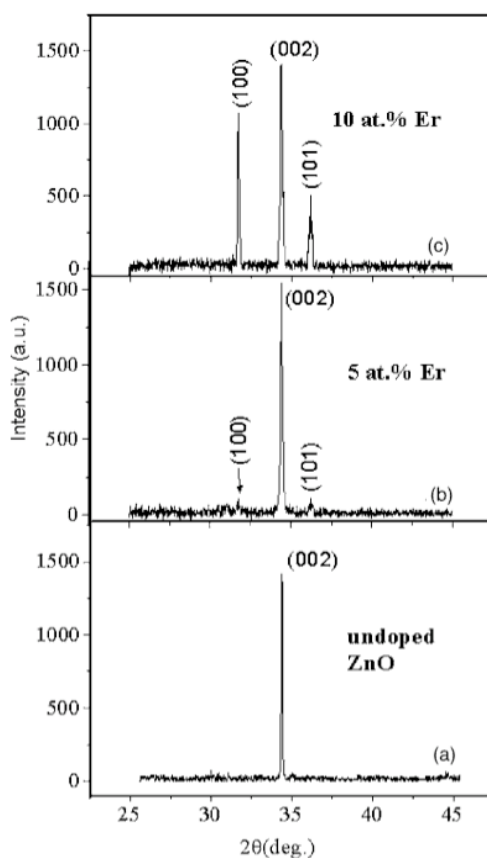

Fig. 17. X-ray diffractograms of ZnO Films: (a) Undoped ZnO (b) Er-doped ZnO 5 at. %, (c) 10 at. %.

The study of the samples composition leading to the results of Table 3 denotes the almost entire recovering of erbium proportion of the spraying bath in Er–ZnO samples, which raises the problem of the dopant insertion mode. Due to the difference in the valence charge [Zn(II) and Er(III)] and the ionic radius, [$R_i(Er^{3+}) \cong 0.09$ nm and $R_i(Zn^{+2}) \cong 0.074$ nm], Er is more likely to be interstitial than substitutional in ZnO matrix. On the other hand, the increase of Er content in the doped samples goes together with a decrease of Zn /O ratio. That indicates an increase of oxygen defects in ZnO lattice that is expected to favor the building of Er–O complexes of some interest in the study of the IR emissions of the material.
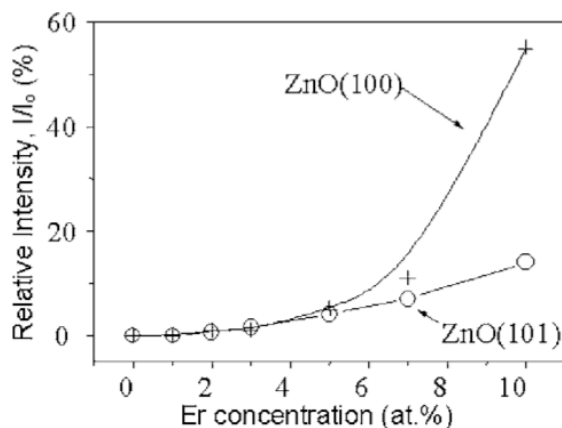

Fig. 18. Relative integrated intensity I/Io of the 100 and 101 x-ray peaks measured from the intensity Io of the 002 peak with respect to Er content in the investigated samples.

Bath composition [Zn^{-2}, Er^{+3}] (M)	Zn (at. %)	O (at. %)	Er (at. %)	Zn/O	Cl (at. %)	S (at. %)	C, Si, Be (at. %)
[0.05,0.00]	47.80	47.50	0.00	1.006	2.20	1.60	0.89
[0.049,0.001]	45.57	47.30	2.23	0.963	1.93	1.95	1.02
[0.047,0.003]	42.93	46.25	4.87	0.928	1.85	2.90	1.20
[0.045,0.005]	37.65	46.70	10.15	0.815	1.73	2.61	1.11

Table 3. Compositional feature of the investigated Er doped ZnO films deposited a constant flow rate value f = 5 ml min^{-1}.

The presence of dopant greatly affects the films surface morphology as depicted in the SEM images of Fig.19. If the undoped sample image in the inset of Fig.19 (a) exhibits regular hexagonal-like grains; the insertion of Er species in ZnO matrix engenders variously shaped crystallites, as appearing in Figs. 19a–19c. Besides, one sees that the sample's mean grain size D determined by the Debye-Scherrer broadering method from the main (002) diffraction peak 21 is greatly affected by the Er content. The corresponding D =f (Er at. %) curve of Fig. 4 shows that D tremendously increases from 1% concentration onwards, the D value of the undoped sample being slightly higher than that obtained at this particular concentration.
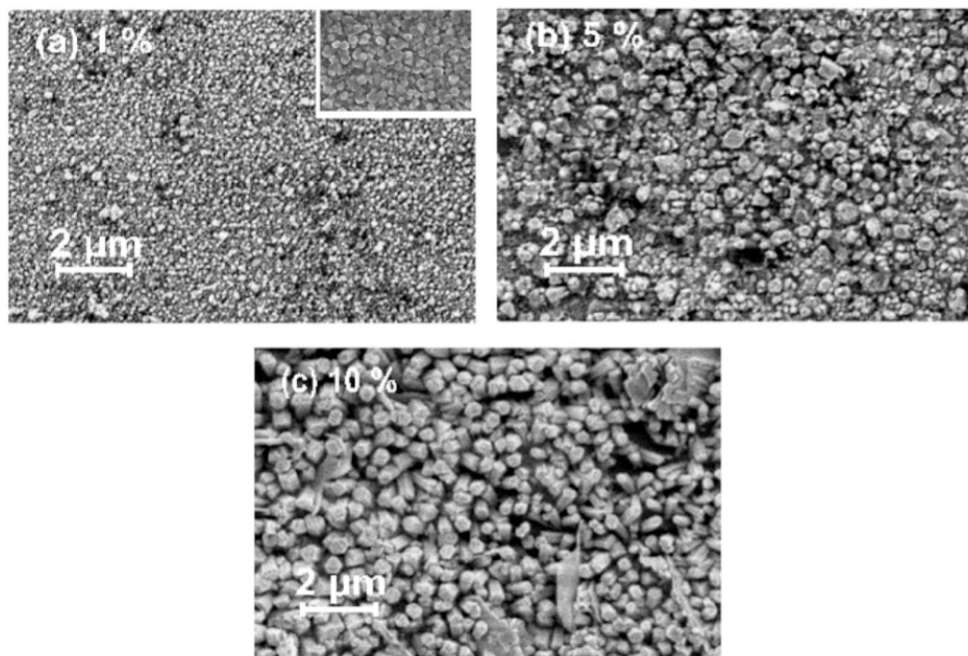
Fig. 19. SEM images of Er-doped ZnO films collected under the incident electron beam energy Eo = 4 keV: (a) for 1 at. %, (b) for 5 at. %, and (c) for 10 at. % Er concentrations. The inset of image (a) depicts the undoped ZnO film's micrograph at the same scale, as proposed in Ref. [44].
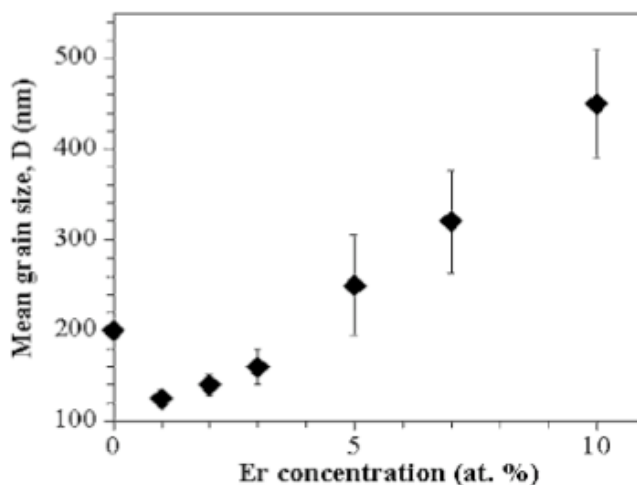

Fig. 20. Dependence of the mean grain size (D) extracted from the SEM images on the sample Er concentration.

4.4 CL– Spectral study of the investigated films

4.4.1 Qualitative CL– Spectral study of the investigated films

The changes observed in the general profile of the CL spectrum linked to the investigated samples give the first indications on the effect of the selected parameters. Referring to the undoped sample result and the common electron beam energy E_0=5 KeV, one can see in Fig.21 that the evolution of the sample CL-spectral profile somewhat deviates from the regular insertion of Er in ZnO matrix. In actual fact, it clearly appears that the spectrum of the Er 1 at. %_-doped ZnO specimen exhibits only the near UV emission peak of 382 nm wavelength. This greatly differs from the result of the other samples for which at least one supplementary peak appears in the visible region. Since these supplementary emission peaks exist for both the undoped and the Er 2 at. % ZnO samples, one infers the occurrence of a specific phenomenon in the material for 1 at. % Er. This phenomenon reflects a deactivation and a reactivation of the peaks, respectively, centered at 440, 520, and 650 nm, below and beyond this particular Er concentration. These peaks are frequently known to be characteristic of the undoped ZnO CL spectrum [45]. All of them are commonly assigned to structural defects, their individual mechanism being not yet clearly identified. The green emission of 520 nm wavelength is currently associated with either Zn or O defect or excess [31].

The result in Table 3 regarding this sample confirms the as expected non stoichiometry feature since it corresponds to the ratio Zn/O=1.006. The observed oxygen defect of the material can be presumably compensated during the film formation by the oxygen-rich phase of the Er_2O_3 deposition solution, the related Er content 1 at. % being marginal. This compensation, directly depending on the defects rate of the undoped sample, is expected to engender deactivation of the green emission as observed here before Er 1 at. % concentration. The increase of Er in ZnO matrix favors the selective excitations of Er^{+3} ions indirectly due to the electron-hole _e-h_ intermediate process via ZnO host, as explained in Ref [46]. This appears as the main cause of the spectral results for Er content higher than 1 at. % for which the inner shell transitions of the Er^{3+} ions engender the emitted peaks. In that case, practically the same visible bands than the undoped ZnO sample are obtained due to the radiative mechanisms from different excited states to the ground state $I_{15/2}$. 4F5/2 excited state originates the peak centered at 455 nm, while $^2H_{11/2}$ and $^4F_{9/2}$, respectively, lead to the 526 and 665 nm emissions.

Assuming that the effect of the electron beam energy on the investigated sample is similar regardless of the doping concentration, the study is here proposed from a Er 5 at. % doped specimen. In that case, Fig.22 reveals two main observations: (i) some of the typical CL peaks appear only with the increase of Eo value, which is clearly depicted comparing spectra (a) and (f). The modification obtained can be explained by a deeper penetration of the incident electrons in the material that increases the rate of all the shell electronic transitions of Er^{+3} described above as being responsible for the main peaks obtained in the visible region. We point out that the near UV emission of 385 nm characteristic of the excitonic band edge of pure ZnO material is free of doping, and hence is only affected by this general beam electron penetration that should be the origin of the increase of its peak's intensity. (ii) The results obtained shows that E_o differently affects the as-obtained CL peaks. In actual fact, it clearly appears that the transition from the $(H_{11/2})$ excited states linked to

the 526 nm emission peak is predominantly involved in the E_o increase even though those from the $(F_{5/2})$ and $(F_{9/2})$ states, respectively, related to 455 and 665 nm, also remain important. The regular increase of all these peaks intensity contrasts with the appearance of specific emissions linked to particular excitation energy values observed in the photoluminescent results of Er doped ZnO thin films reported by Komuro et al [47].
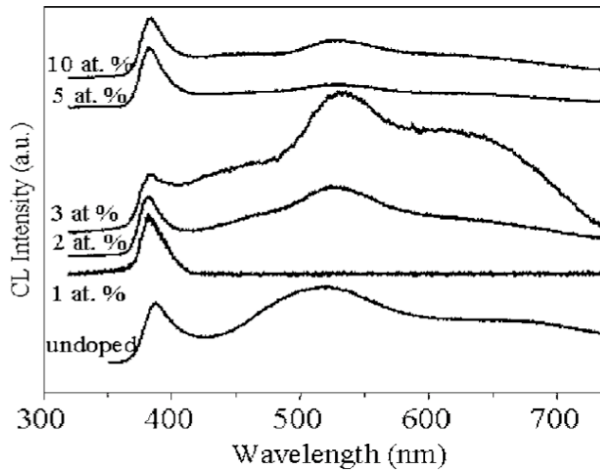

Fig. 21. Dependence of the CL-spectral characteristics of the undoped and Er-doped ZnO films on the sample's Er concentration obtained at the incident electron beam energy E= 10 keV.
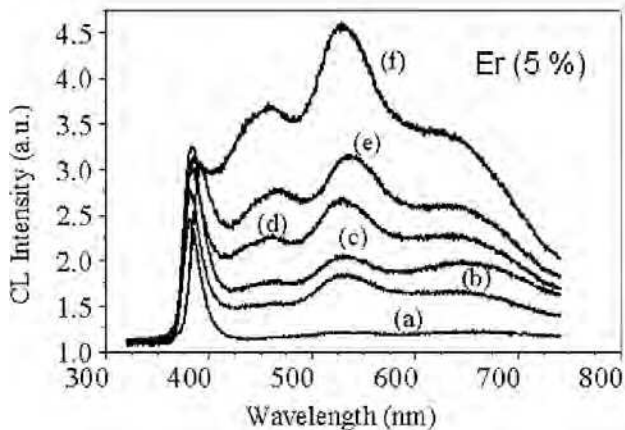

Fig. 22. Dependence of the CL spectral characteristics of Er(5 at. %)-doped ZnO sample on the incident electron beam energies: (a) for Eo = 4 keV, (b) for Eo = 5 keV, (c) for Eo = 7 keV, (d) for Eo = 10 keV, (e) for Eo = 15 keV, and (f) for Eo = 20 keV.

We point out that the broadening of the CL spectral peaks in Figs. 21 and 22 is likely to be connected with electronphonon interactions. This is a characteristic of disordered media in the range of the ZnO band gap (1.5–3.5 eV), particularly under the Er doping effect. [48]

4.4.2 Integration and normalized intensity of the CL – Spectral peaks

An accurate study of a luminescent spectrum requires taking into account the possible peak's overlap phenomenon. This is currently overcame by a spectral modeling leading to a better peak's integration that remains necessary for the assessment of their relative intensity. The application of Gaussian model, as shown in Fig.23, appears to be more appropriate here. The reported result shows that the typical four CL peak feature of the Er doped ZnO material obtained with spectra Figs. 21 and 22 remains unchanged in the modelling despite the shape modification caused by the incident electron beam energy. With the near UV emission being free of the doping process, only the evolution of the three visible CL peaks mentioned above as centered at 445, 526, and 665 nm wavelengths, respectively, can be studied with respect to Er content in ZnO material. Besides, their intensity can lead to examine the effect of the incident electron beam energy for every Er-doped ZnO sample in the region higher than 1 at. %. The normalization of their respective intensity from the one of the near UV value leads to a better assessment of the doping and the incident energy influences.
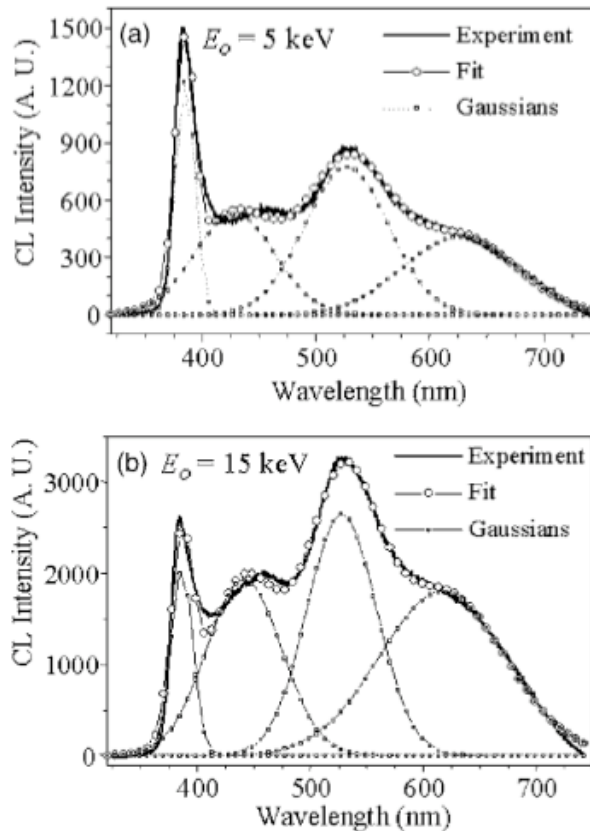

Fig. 23. Gaussian decomposition of CL spectra related to the Er (5 at. %)-doped ZnO sample for two different incident electron beam energies: (a) for E= 5 keV and (b) for E= 15 keV.

The results of Fig.24 show that, for a constant incident electron beam E_o=10 KeV, the increase of Er content in ZnO matrix leads to different peaks intensity profiles. However, a common increasing trend is observed till 3 at. % Er content. This concentration corresponds to a maximum for the intensities of the violet 445 nm and green 526 nm emissions. In both cases, a decrease is observed from this Er percentage towards a plateau neatly appearing at nearly 5 at. %. No decrease is obtained for the red emission 665 nm whose plateau onset is 3 at. % with a higher intensity value. One infers from these results that the radiative mechanism from the excited state $F_{9/2}$ to the ground state $I_{15/2}$ is quite predominant in the investigated Er concentration region. The lowering in the rate of the radiative mechanisms from the $F_{5/2}$ and $H_{11/2}$ excited states to $I_{15/2}$ linked to the 445 and 526 nm peak's intensities might have a link to be clarify with either the reported textural change of Fig.17 occurring at Er concentration higher than 3 at. % or the material composition. Since this material texture remains unchanged below this concentration, the regular increase of the three CL peaks intensity in this region is likely to be the fact of a regular increase of all the radiative mechanisms involved going together with the increase of the active Er species in the material.

The similarity of the electron beam energy effect on the investigated samples assumed above is here confirmed in Fig.25 from the study of samples having three different Er contents. It appears in every case that the increase of E_o leads to that of the normalized intensity of the green emission peak of 526 nm. We point out that the same increasing trend is observed with the violet and red emissions of 445 and 665 nm. As already mentioned, this result has a direct connection with the irradiated volume of the material due to further Er ions involved. A saturation regime is expected at higher E_o value, the related current being mostly affected by the sample Er content and possibly by the textural change observed between 2 and 10 at. %.
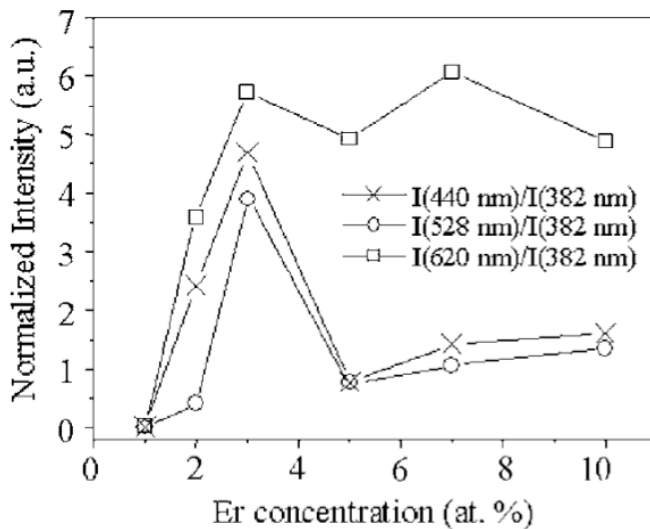

Fig. 24. Normalization (from the UV band) of the integrated intensity related to the main emission peaks and its dependence on the sample Er concentration for E= 10 keV.
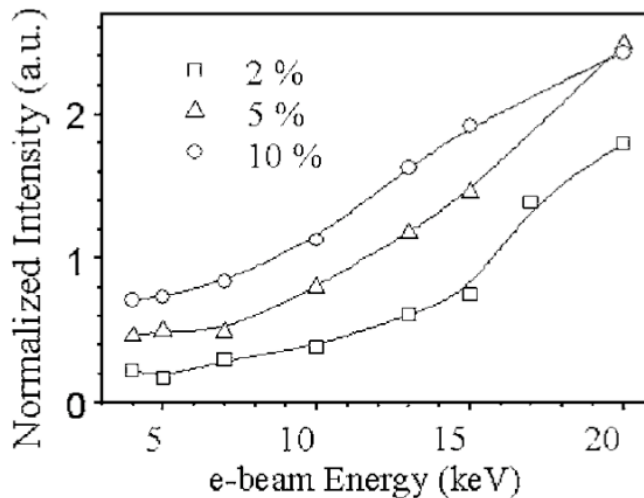
Fig. 25. Normalization (from the UV band) of the integrated intensity related to the green emission peak (λ = 526 nm) and its dependence on the incident electron beam energy for three different samples Er concentration.

4.4.3 CL imaging and repartition of the emitting centers

The study is here performed with a Er 5 at. % doped ZnO sample under an incident beam energy E_o=5 KeV being agreed that the results are similar regardless of the doping concentration and E_o value. The CL images are collected at a required wavelength having a 16 nm spectral bandwidth. Figure 10 depicts those obtained from each of the main emitted wavelengths of the material, the dark mark surrounded by a dashed line in some pictures just serves for the positioning of the investigated sample zone. Figure 10-a related to the UV band edge λ =382 nm clearly shows that the luminescent emitting centers of this particular wavelength are regularly dispersed all over the material, merging with the material surface grains. Being free of doping, such a repartition of emitting centers is easily explained since only ZnO matrix is here concerned. It could be noted that the CL image as obtained is the neatest one due to the predominant intensity of the related peak as it appears in Fig.21. The emitting centers' image of the green wavelength λ =526 nm proposed in Fig.26-b shows that the grain like feature is once again recovered. One infers that Er species are well localized in the surface grains. The result in Fig. 26-c obtained for the red line λ =665 nm greatly contrasts with the two precedent investigated wavelengths since the emitting centers are not clearly distinguished, the intensity signal being quite negligible in Fig. 21. The relationship between the Er species repartition and the emitting centers is thereby difficult to be established. Probably, a better result could be expected for this wavelength at higher incident energy values.
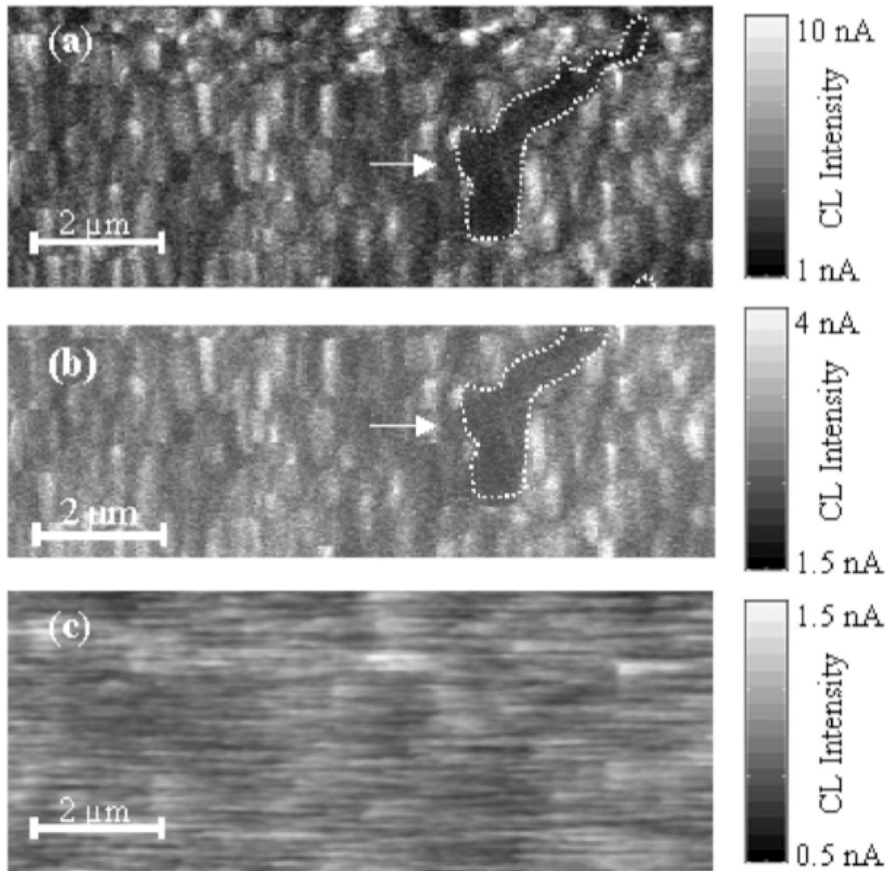
Fig. 26. Monochromatic CL images of the Er (5 at. %)-doped ZnO films collected at $E_0 = 5$ keV, with a focalized spot of 5 nm diameter: (a) for $\lambda=382 \pm 8$ nm, (b) for $\lambda=526 \pm 8$ nm, and (c) for $\lambda=665 \pm 8$ nm wavelengths.

5. Summary and conclusion

It comes out of the present work that the role of heavy elements as lanthanides in the doping of ZnO material has not yet been quite explored. Dealing here with Er species inserted in this material matrix, we find that the increase of erbium concentration leads to some textural change in the growth of Er–ZnO film. A single$\square$002$\square$ preferred growth orientation is obtained at lower Er contents, while the$\square$100$\square$and$\square$101 additional ones become neatly perceptible from about 5 at. % Er concentration. Restricting our luminescence study in the near UV and visible regions, we show that Er concentration greatly affects the CL-spectral feature of the material. All the visible emitted bands entirely disappear for 1 at. % Er concentration. In the investigated wavelength region, the normalization of the main visible peaks intensity from that of the UV peak shows that the radiative transitions in the Er^{+3} ion shell from the F9/2 excited states to I15/2 ground state,

responsible for the 665 nm emitted band, are always predominant in the material. Both, the green λ=526 nm and the violet λ=445 nm emitted bands exhibit a maximal normalized intensity for 3 at. % Er concentration that is followed by a lowering and stabilization reached beyond 5 at. % Er content.

6. Conclusion

The dependence of cathodoluminescence properties of spray-deposited ZnO films on process parameters such as substrate temperature, airflow rate and precursors, has been studied in detail. We have found that the luminescence intensity depend strongly on process parameters. The optimum values of substrate temperature and airflow rate have been determined to give the best luminescent ZnO films.

The produced films at optimum condition exhibit luminescence characteristics comparable to films grown by more sophisticated techniques. These films may be useful for specific applications as transparent n-type windows in solar cells or for sensors devices where large surface areas are needed and may also be an important candidate for UV diode lasers applications.

It seems here evident that the particular spectral feature of the single emitted near UV band obtained for 1 at. % Er content in ZnO matrix can be of prime interest in the technology of low cost light emitting diodes LEDs.

7. References

[1] Cowley. J.M. (1969)- Image contrast in a transmission scanning electron microscope. Appl. Phys. Lett., 15, 58.

[2] Z.C. Jin, J. Hamberg, C.G. Granqvist, J. Appl. Phys. 64(1988) 5117.

[3] J.B. Yoo, A.L. Fahrenbruch, R.H. Bube, J. Appl. Phys. 68(1990) 4694.

[4] Y. Chen, D.M. Bagnall, H. Foh, K. Park, K. Hiraga,Z. Zhu, T. Yao, J. Appl. Phys. 84 (1998) 3912.

[5] E. Jeff, Nause, III-Vs Review 12 (1999) 28.

[6] Y. Chen, D.M. Bagnall, T. Yao, Mater. Sci. Eng. B 75(2000) 190.

[7] Y.C. Kong, D.P. Yu, B. Zhang, W. Fang, S.Q. Feng,Appl. Phys. Lett. 78 (2001) 407.

[8] R. Menner, B. Dimmler, R.H. Maunch, H.W. Shock,J. Crystal Growth 86 (1988) 906.

[9] C.Y. Lee, Y.K. Su, S.L. Chen, J. Crystal Growth 96 (1989)785.

[10] A. Sarkar, S. Chaudhuri, A.K. Pal, Phys. Stat. Sol. (A) 119(1990) K21.

[11] T. Minamai, T. Yamamoto, T. Miyata, Thin Solid Films366 (2000) 63.

[12] K. Haga, F. Katahira, H. Watanabe, Thin Solid Films 344(1999) 145.

[13] Y. Natsume, H. Sakata, T. Hirayama, H. Yanigida,J. Appl. Phys. 72 (1992) 4203.

[14] M. Ruth, J. Tuttle, J. Goral, R. Noufi, J. Crystal Growth96 (1989) 363.

[15] A. Ortiz, C. Falcony, J. Hernandez, M. Garcia,J.C. Alonso, Thin Solid Films 293 (1997) 103.

[16] A. Maldonado, R. Asomoza, J. Canetas-Ortega,E.P. Zironi, R. Hernandez, O. Solorza-Feria,Sol. Energ. Mater. Sol. Cells 57 (1999) 331.

[17] S.A. Studenikin, M. Cocivera, W. Kelner, H. Pascher,J. Lumin. 91 (2000) 223.

[18] M. de la, L. Olvera, A. Maldonado, R. Asomoza,O. Solorza, D.R. Acosta, Thin Solid Films 394 (2001) 242.

[19] N. Benhamdane, W.A. Murad, R.H. Misho, M. Ziane,Z. Kebbab, Mater. Chem. Phys. 48 (1997) 119.

[20] S.A. Studenikin, N. Golego, M. Cocivera, J. Appl. Phys.83 (1998) 2104.

[21] M. Addou, A. Moumin, B. El idrissi, M. Regragui, A.Bougrine, A. Kachouane, J. Chem. Phys. 96 (2) (1999) 232.

[22] F. Paraguay, D.J. Morales, W. Estrada, L.E. Andrade,M. Miki-Yoshida, Thin Solid Films 366 (2000) 16.

[23] H.J. Egelhaaf, D. Oelkrug, J. Crystal Growth 161 (1996)190.

[24] T. Sekiguchi, N. Ohashi, Y. Terada, Jpn. J. Appl. Phys.Part 2 Lett. 36 (1997).

[25] P. Fons, K. Iwata, S. Niki, A. Yamada, K. Matsubara,J. Crystal Growth 201/202 (1999) 627.

[26] H. Nanto, T. Minami, S. Takata, Phys. Status Solidi A 65(1981) K131.

[27] J. Zhong, A.H. Kitai, P. Mascher. J. Electrochem. Soc. 140(1993) 3644.

[28] K. Vanheusden, W.L. Warren, C.H. Seager, D.R. Tallant,J.A. Voigt, B.E. Gnade, J. Appl. Phys. 79 (1996) 7983.

[29] P. Scherrer, Goettinger Nachr 2 (1918) 98.

[30] R. Dingle, Phys. Rev. Lett. 23 (1969) 579.

[31] K. Vavheusden, C.H. Seager, W.L. Warren, D.R. Tallant,J.A. Voigt, Appl. Phys. Lett. 68 (1996) 403.

[32] E.G. Bylander, J. Appl. Phys. 49 (1978) 1188.

[33] T. Minami, H. Nanto, S. Takata, J. Lumin. 24/25 (1981)63.

[34] C. Falcony, A. Ortiz, M. Garcia, J.S. Helman, J. Appl.Phys. 63 (1998) 7.

[35] A. Mitra, R.K. Thareja, V. Ganesan, A. Gupa, P.K.Sahoo, V.N. Kulkarni, Appl. Surf. Sci. 174 (2001) 232.

[36] K. Lohnert, E. Kubalek, Microscopy of SemiconductingMaterials, Institute Of physics Publishing, Bristol, 1983,

[37] M. Troyon, D. Pastre, J.P. Jouart, J.L. Beaudoin, Ultramicroscopy75 (1) (1998) 15.

[38] I. Shin, C.V. Qin, J. Appl. Phys. 58 (1985) 2400.

[39] S.A. Studenikin, N. Golego, M. Cocivera, J. Appl. Phys. 84 (1998) 4.

[40] H.J. Egelaaf, D. Oelkrug, J. Cryst. Growth 161 (1996) 190.

[41] K. Lohnert, E. Kubalek, Microscopy of Semiconducting Materials,IOP, Bristol, (1983) 303.

[42] M. Kolhs, M. Bonanni, L. Spanhel, D. Su, and M. Giersig, Appl. Phys. Lett. 81, (2002) 3858

[43] X. T. Zhang, Y. C. Liu, J. G. Ma, Y. M. Lu, D. Z. Shen, W. Xu, G. Z. Zhong, and X. W. Fan, Thin Solid Films 413, (2002) 257 .

[44] A. El Hichou, A. Bougrine, J.-L. Bubendorff, J. Ebothé, M. Addou, and M. Troyon, Semicond. Sci. Technol. 17, (2002) 607

[45] C. Shi, Z. Fu, C. Guo, X. Ye, Y. Wei, J. Deng, J. Shi, and G. Zhang, J. Electron Spectrosc. Relat. Phenom. 101–103, (1999) 629.

[46] X. T. Zhang, Y. C. Liu, J. G. Ma, Y. M. Lu, D. Z. Shen, W. Xu, G. Z. Zhong, and X. W. Fan, Thin Solid Films 413, (2002) 257.

[47] S. Komuro, T. Katsumata, T. Morikawa, X. Zhao, H. Isshiki, and Y. Aoyagi, J. Appl. Phys. 88, (2000) 7129.

[48] I. V. Kityk, J. Wasylak, D. Dorosz, J. Kucharski, S. Benet, and H. Kaddouri, Opt. Laser Technol. 33, (2001) 511.
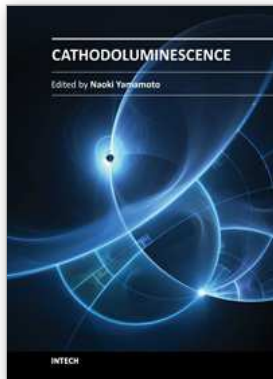
Cathodoluminescence

Edited by Dr. Naoki Yamamoto

Cathodoluminescence (CL) is a non-destructive technique to characterize optical and electronic properties of nanostructures in many kinds of materials. Major subject is to investigate basic parameters in semiconductors, impurities in oxides and phase determination of minerals. CL gives information on carrier concentration, diffusion length and life time of minority carriers in semiconductors, and impurity concentration and phase composition in composite materials. This book involves 13 chapters to present the basics in the CL technique and applications to particles, thin films and nanostructures in semiconductors, oxides and minerals. The chapters covered in this book include recent development of CL technique and applications to wide range of materials used in modern material science.

How to reference

In order to correctly reference this scholarly work, feel free to copy and paste the following:

M. Addou, J. Ebothé, A. El Hichou, A. Bougrine, J.L. Bubendorff, M. Troyon, Z. Sofiani, M. EL Jouad, K. Bahedi and M. Lamrani (2012). Cathodoluminescence Properties of Zno Thin Films, Cathodoluminescence, Dr. Naoki Yamamoto (Ed.), ISBN: 978-953-51-0362-2, InTech, Available from:
http://www.intechopen.com/books/cathodoluminescence/cathodoluminescence-properties-of-zno-thin-films-

INTECH
open science | open minds